

Complete decoupling of magnetic order and superconductivity in a conventional superconductor

D. G. Mazzone,^{1,*} R. Sibille,² M. Bartkowiak,² J. L. Gavilano,¹ C. Wessler,²
M. Månsson,^{1,†} M. Frontzek,^{1,‡} O. Zaharko,¹ J. Schefer,¹ and M. Kenzelmann^{2,§}

¹*Laboratory for Neutron Scattering and Imaging,
Paul Scherrer Institut, 5232 Villigen PSI, Switzerland*

²*Laboratory for Scientific Developments and Novel Materials,
Paul Scherrer Institut, 5232 Villigen PSI, Switzerland*

(Dated: November 19, 2021)

Superconductivity and magnetic order strongly compete in many conventional superconductors, at least partly because both tend to gap the Fermi surface. In magnetically-ordered conventional superconductors, the competition between these cooperative phenomena leads to anomalies at magnetic and superconducting phase boundaries. Here we reveal that in Pr₂Pt₃Ge₅ superconducting and multiple magnetic order are intertwined within the same *HT*-phase space, but remain completely decoupled. Our thermal conductivity measurements provide evidence for normal electrons in the superconducting phase from which magnetic order emerges with negligible coupling to electron bands that contribute to superconductivity.

PACS numbers: 74.70.Dd, 75.20.Hr, 75.30.Kz

I. INTRODUCTION

The coexistence of magnetic order and superconductivity has been investigated ever since Ginzburg theoretically studied the possibility of ferromagnetic superconductors over half a century ago [1]. While strong magnetic spin fluctuations are present and play an important role in many unconventional superconductors [2–4], magnetic correlations compete strongly with conventional superconductivity. In clean metals even a 1% concentration of magnetic impurities can result in a complete loss of conventional superconductivity [5].

Coexistence of magnetic order and conventional superconductivity has been observed in metallic materials featuring localized magnetic moments. In such systems, the magnetic ions are well isolated from the electrons of the conduction bands and the direct exchange between the magnetic ions and the electrons at the Fermi level is weak. This reduces scattering of Cooper pairs so that conventional superconductivity and magnetism can coexist [6, 7]. Magnetic superconductivity was first found in *RMo₆S₈*, *RMo₆Se₈*, *RRh₄B₄* and *RNi₂B₂C* (with *R* being selected rare-earth elements) [8–14]. The competition between localized magnetism and superconductivity gives rise to exotic phenomena, such as reentrant superconductivity and anomalous upper critical fields [15–17]. Competition between magnetism and superconductivity arises from magnetostatic interactions and from competition of electron states at the Fermi surface, making it

difficult to find materials where conventional superconductivity and magnetic order do not compete. In this article, we demonstrate that in Pr₂Pt₃Ge₅ the magnetic and superconducting properties are completely decoupled. We identify Pr₂Pt₃Ge₅ as a unique conventional superconductor where magnetic order and conventional superconductivity do not compete. It is thus a good model magnetic superconductor to selectively study interactions leading to magnetic order and conventional superconductivity in the same material.

Pr₂Pt₃Ge₅ belongs to the family of compounds with the general formula *R₂M₃X₅*, where *R* is a rare-earth element, *M* a transition metal and *X* a *s-p* metal [18–23]. The crystal structure is satisfactorily refined in the space group *Ibam* with lattice constants $a = 10.13 \text{ \AA}$, $b = 11.86 \text{ \AA}$ and $c = 6.23 \text{ \AA}$ [18]. At zero field, Pr₂Pt₃Ge₅ displays a transition at relatively high temperature, $T_c = 7.8 \text{ K}$, where a macroscopic fraction of the sample condensates into a superconducting phase. Transport measurements suggest that Pr₂Pt₃Ge₅ is a multiple gap conventional superconductor with a Curie-Weiss temperature of $T_{CW} \approx -40$ and -55 K for $\vec{H} \parallel c$ and $\vec{H} \parallel ab$, respectively. Additionally, two antiferromagnetic (AF) transitions at $T_{N_1} = 3.5 \text{ K}$ and $T_{N_2} = 4.2 \text{ K}$ are found inside the superconducting condensate [18].

I. RESULTS AND DISCUSSION

A. Experimental details

Single crystals were synthesized using a Pt-Ge mixture as self-flux [18]. High purity elements (with atomic parts of 1 Pr, 4 Pt and 20 Ge) were placed in an alumina crucible and heated to 1130 °C in an evacuated and sealed quartz tube. After 40 hours the liquid was cooled to 850 °C at a rate of 3 °C/h. The crystals were separated by means of a centrifuge using quartz wool as a filter. Typical single crystals showed RRR values of 5 and a consistent superconducting volume fraction $v_s \approx 30\%$, measured via magnetization measurements upon applying 1 mT along [001].

Electrical resistivity, magnetization and neutron diffraction were measured on the same single crystal of size $1.2 \times 1.2 \times 5.3 \text{ mm}^3$ and mass $m \approx 64 \text{ mg}$. The single crystal used for thermal conductivity measurements had a mass of $m \approx 12 \text{ mg}$ with a shape of $0.7 \times 0.9 \times 3.35 \text{ mm}^3$. Electrical resistivity measurements were performed using a four-probe method in a Quantum Design PPMS. Magnetization data were recorded for magnetic fields $\mu_0 H = 0 - 7 \text{ T}$ with $\vec{H} \parallel [100]$, $[010]$ and $[001]$ using a Quantum Design MPMS-XL SQUID magnetometer. Simultaneous measurements of the resistivity and the magnetization were made in the MPMS magnetometer. Thermal conductivity results were obtained using the one-heater-two-thermometer steady-state method. The heat current was fixed along the crystallographic [001] direction, whereas the magnetic field could be rotated in the ab -plane. In order to exceed the superconducting critical field of indium solder joint that affixed the crystal to the thermal base, conductivity was measured at a minimal field of $\mu_0 H = 50 \text{ mT}$ at temperatures below 1 K. Single crystal neutron scattering was performed using the diffractometers DMC and TriCS as well as on the triple-axis spectrometer TASP at the Swiss Spallation Neutron Source (SINQ) at the Paul Scherrer Institut, Villigen, Switzerland. Diffraction experiments on DMC were carried out between $T = 1.8 - 10 \text{ K}$ with a neutron wavelength $\lambda = 3.808 \text{ \AA}$. The investigations on TriCS were performed with $\lambda = 2.316$ and 1.175 \AA in a temperature range $T = 1.7 - 10 \text{ K}$ using either a 4-circle cryostat with a Joule-Thompson insert or a vertical 6 T magnet for fields applied along [001]. Diffraction studies on TASP were carried out with $\lambda = 2.36 \text{ \AA}$ between $T = 1.6 - 10 \text{ K}$ and for fields $\mu_0 H = 0 - 3 \text{ T}$ with $\vec{H} \parallel [100]$. The magnetic structures were refined using FULLPROF [24].

B. Superconducting properties

Fig. 1 displays the temperature dependence of the upper critical field, $H_{c2}(T)$, for $\vec{H} \parallel [100]$, $[010]$ and $[001]$

obtained from field dependent resistivity measurements. At zero field a superconducting transition temperature $T_c = 7.8 \text{ K}$ is found (see inset of Fig. 1), in agreement with earlier reports [18]. At low temperatures the upper critical field saturates at $\mu_0 H_{c2}(0) \approx 1.6 \text{ T}$. The orbital limiting field of the superconducting condensate is estimated from the slope of the $\mu_0 H_{c2}(T)$ near T_c using $\mu_0 H_{c2}^{orb}(0) = -0.73 |dH_{c2}/dT|_{T_c} T_c = 1.5(1) \text{ T}$ [25]. This leads to a Ginzburg-Landau coherence length of $\xi_0 \approx 148(5) \text{ \AA}$ using $\mu_0 H_{c2}(0) = \Phi_0/2\pi\xi_0^2$, with Φ_0 the magnetic flux quantum [26, 27]. On contrary, the Pauli limiting field is calculated as $\mu_0 H_{c2}^P(0) = \Delta/\sqrt{g}$, where g is the Lande factor and Δ the superconducting gap [27]. Taking into account the reduced superconducting gap revealed by the heat capacity jump at T_c ($\Delta C/\gamma T_c = 0.36$ compared to the BCS value of 1.43 in isostructural $\text{La}_2\text{Pt}_3\text{Ge}_5$), the lower boundary of the Pauli limiting field in $\text{Pr}_2\text{Pt}_3\text{Ge}_5$ is approximated as $\mu_0 H_{c2}^P(0) \approx 3.6 \text{ T}$ [18, 27]. Thus, the system is characterized by an orbital limiting superconductor with an isotropic upper critical field, $H_{c2}(T)$.

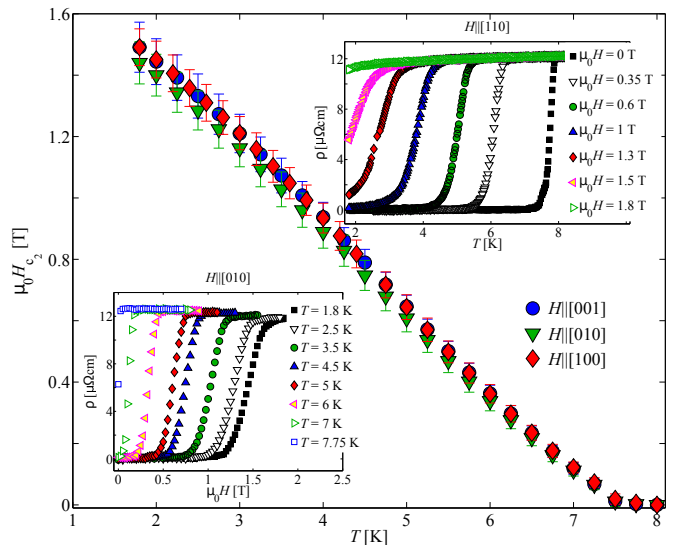


FIG. 1: Temperature dependence of the upper critical field, $H_{c2}(T)$, measured via electrical resistivity. The insets show electrical resistivity data as a function of the temperature and magnetic field, respectively.

The low-temperature thermal conductivity divided by the temperature, $\kappa(T)/T$, in the superconducting and normal state is shown in Fig. 2a. In the inset of Fig. 2a κ/T is plotted against T^2 . At very low temperatures the electron and phonon contribution of the thermal conductivity, $\kappa = \kappa_e + \kappa_{ph}$, are described by $\kappa = aT + bT^3$. The best fit to the data reveals $b = 0.109(8) \text{ W/K}^4\text{m}$ and $a = 0.1314(5) \text{ W/K}^2\text{m}$ at $\mu_0 H = 50 \text{ mT}$. The non-vanishing electron contribution of the thermal conductivity at lowest temperatures suggests either nodal superconductivity or the presence of normal state electrons

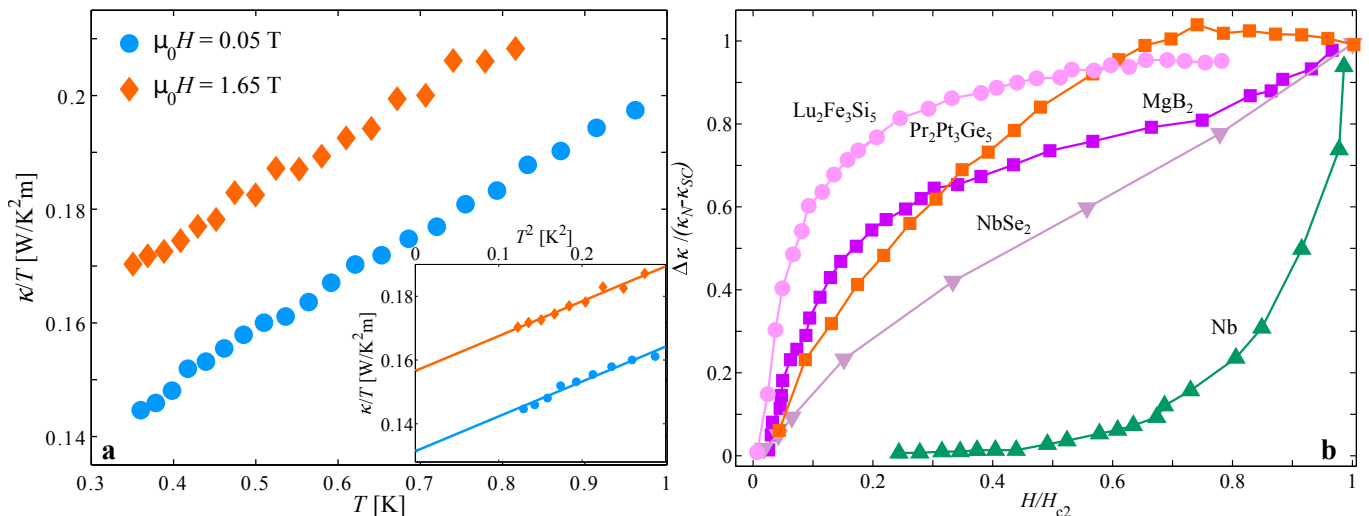


FIG. 2: (a) Temperature dependence of the thermal conductivity in the superconducting and normal state. (b) Field dependence of $\Delta\kappa/(\kappa_N - \kappa_{SC}) = (\kappa(H) - \kappa_{SC})/(\kappa_N - \kappa_{SC})$ in $\text{Pr}_2\text{Pt}_3\text{Ge}_5$ and comparison with single and multiple gap superconductors.

within the superconducting condensate. The second scenario can occur when not all electron bands develop a Fermi surface gap at the superconducting transition. Since $\text{Pr}_2\text{Pt}_3\text{Ge}_5$ is a superconductor with an isotropic upper critical field we attribute the non-vanishing residual thermal conductivity to conduction bands that do not contribute to superconductivity. The comparison of $\kappa_e(50$ mT) with $\kappa_e(1.65$ T) suggests that only 16.1(3)% of the density of states is gapped below T_c . We point out that in the structurally related ternary iron silicates it has also been suggested based on specific heat measurements that electron bands remain normal in the superconducting state [28].

The field dependence provides further insight in the symmetry of the superconducting order parameter. We define $\Delta\kappa = \kappa(H) - \kappa_{SC}$ where κ_{SC} denotes the thermal heat conductivity in the superconducting phase at minimal magnetic field, and κ_N the thermal conductivity for $H = H_{c2}$. Fig. 2b shows $\Delta\kappa/(\kappa_N - \kappa_{SC})$ of $\text{Pr}_2\text{Pt}_3\text{Ge}_5$ measured for a fixed temperature, $T = 400$ mK, as a function of magnetic field oriented in the ab -plane. This field dependence is compared with the multiple gap superconductors $\text{Lu}_2\text{Fe}_3\text{Si}_5$, MgB_2 and NbSe_2 as well as the s -wave superconductor Nb [29–32]. The field dependence of the thermal conductivity of $\text{Pr}_2\text{Pt}_3\text{Ge}_5$ is in dramatic contrast to the behavior of Nb , in which small fields hardly affect $\Delta\kappa/(\kappa_N - \kappa_{SC})$. A strong enhancement of $\Delta\kappa/(\kappa_N - \kappa_{SC})$ provides evidence for delocalized quasiparticles as found in multiple gap superconductors (see Fig. 2b). This comparison suggests that $\text{Pr}_2\text{Pt}_3\text{Ge}_5$ is a multigap superconductor and the change of slope suggests an upper critical field of $\mu_0 H_{c2}^s \approx 0.3$ T of the smaller gap.

B. Magnetic properties

Using neutron diffraction we observed magnetic reflections below T_{N1} and T_{N2} at $\vec{Q} = \vec{G} \pm \vec{q}$ with \vec{G} a nuclear wave-vector. Representative data around the reciprocal lattice position $(0, 2, 1)$ are shown in Fig. 3a and b. For $T_{N1} < T \leq T_{N2}$ an incommensurate (ICM) propagation vector $\vec{q}_2 = (0, 1 - \delta, 0)$ with $\delta \approx 0.15$ is found (see inset of Fig 3b). $\delta(T)$ decreases linearly with decreasing temperature for $T_{N1} < T < T_{N2}$ (see inset of Fig 3c). Below T_{N1} the magnetic structure abruptly adopts a commensurate (CM) wavevector, $\vec{q}_1 = (0, 1, 0)$, that breaks the body-centering of the unit cell. The propagation vectors of the CM and ICM structure are reminiscent of the magnetic phases of the isostructural compounds $\text{Tb}_2\text{Ni}_3\text{Si}_5$ and $R_2\text{Ni}_3\text{Si}_5$ ($R = \text{Tb}, \text{Pr}$ and Nd) and $\text{Ce}_2\text{Ni}_3\text{Ge}_5$, respectively [22, 33].

Fig. 3c shows the integrated intensities of the magnetic reflections $(0, 2, 1)$ and $(0, 2 + \delta, 1)$ as a function of temperature. The gradual increase of magnetic intensity of the ICM magnetic structure reveals a second-order phase transition with a critical exponent $\beta = 0.36(1)$ and transition temperature $T_{N2} = 4.10(6)$ K (see black line in Fig. 3c). Therefore, the data suggest a transition belonging to the universality class of either the 3D Heisenberg or the 3D model of XY spins. In contrast we observe a first-order type of transition at $T_{N1} = 3.4$ K. We also find a hysteretic behavior with a small coexistence region of both magnetic structures, $\Delta T \approx 0.15$ K (see Fig. 3a and c) and $\Delta B \approx 60$ mT at $T = 1.6$ K and for $\vec{H} \parallel [100]$.

The crystal structure of $\text{Pr}_2\text{Pt}_3\text{Ge}_5$ is displayed in Fig. 4a. The nearest- and next-nearest-neighbors of the Pr atoms are found in the bc -plane. The mirror plane, orthogonal to the c -axis, restricts the magnetic moment either to the basal ab -plane or along

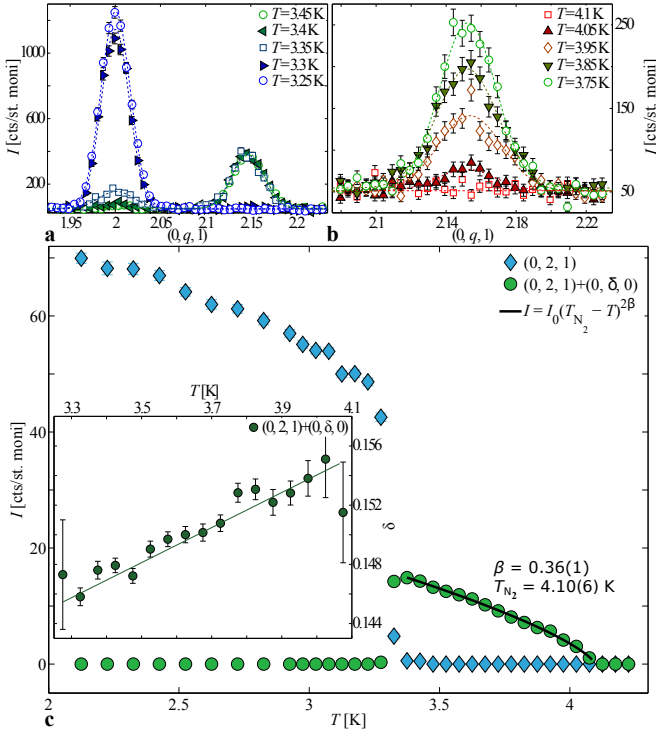


FIG. 3: q -scans of one CM and one ICM magnetic reflection along $(0, q, 1)$ for (a) $3.25 \text{ K} \leq T \leq 3.45 \text{ K}$ and (b) $3.75 \text{ K} \leq T \leq 4.1 \text{ K}$. (c) Temperature dependent integrated intensities of $(0, 2, 1)$ and $(0, 2 + \delta, 1)$. The ICM phase reveals a critical exponent $\beta = 0.36(1)$ and $T_{N_2} = 4.10(6) \text{ K}$. The inset depicts the incommensuration $\delta(T)$ as a function of temperature.

the c -axis. The representational analysis for propagation vector \vec{q}_1 yields eight one dimensional irreducible representations with one magnetic orbit at site $(x, y, z) = (0.26874, 0.36898, 0)$. Similarly, four one dimensional representations with two magnetic orbits, at sites $(x_1, y_1, z_1) = (0.26874, 0.36898, 0)$ and $(x_2, y_2, z_2) = (0.7313, 0.6310, 0)$ were found for propagation vector \vec{q}_2 . The best refinements of the magnetic Bragg peak intensities are obtained for the representations with the complex-valued basis vectors, $\vec{S}_j^{\vec{q}_i}$, shown in Table I (\vec{q}_i denotes the propagation vectors and j the positions of the magnetic atoms). The agreement factors, R_F , equal 4 and 3.5% for the CM and the ICM phase, respectively.

The CM structure refinement at $2.1 \text{ K} = T < T_{N_1}$ reveals a non-collinear AF structure shown in Fig. 4b. The structure displays an ordered magnetic moment of amplitude $\mu = 2.33(1)\mu_B$. The magnetic moments are confined in the crystallographic ab -plane at an angle $\Phi = 65.2(3)^\circ$ with respect to the a -axis. The total magnetic moment is reduced to a maximal amplitude of $\mu = 2.01(2)\mu_B$ at $T = 3.5 \text{ K}$ compared to $T = 2.1 \text{ K}$. The ICM magnetic structure at $T_{N_1} < T = 3.5 \text{ K} < T_{N_2}$ is depicted in Fig. 4c. The refinement evidences an amplitude mod-

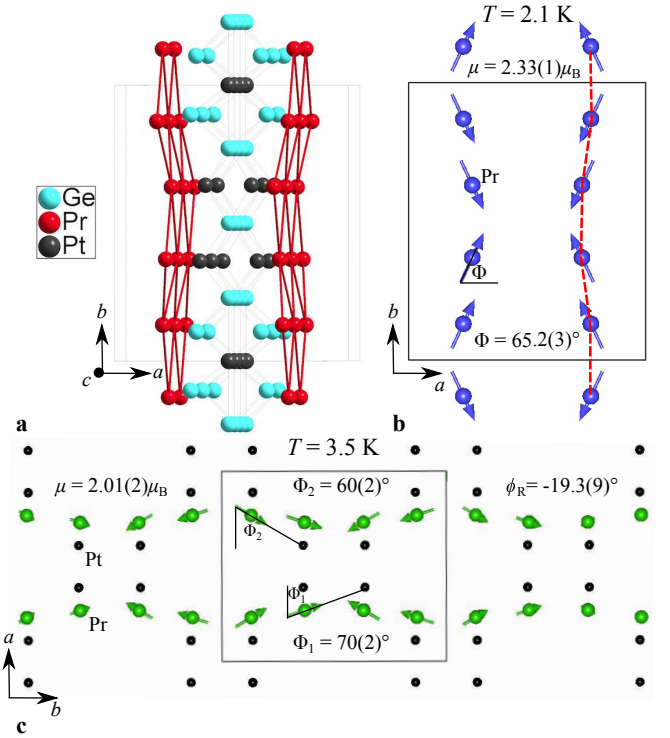


FIG. 4: (a) Crystal structure of $\text{Pr}_2\text{Pt}_3\text{Ge}_5$ with the distorted and buckled square lattice of Pr atoms in the bc -plane. Magnetic structure of (b) the CM and (c) the ICM phase in the ab -plane. The black box denotes the crystallographic unit cell. In the projection along c two consecutive Pr atoms along the red dashed line are at different c -levels. The refinements of the CM and ICM structures reveal a non-collinear antiferromagnetic structure and an amplitude modulated non-collinear antiferromagnetic structure, respectively.

$\vec{S}_1^{\vec{q}_1}$ (x, y, z)	$\vec{S}_2^{\vec{q}_1}$ $(-x, -y, z)$	$\vec{S}_3^{\vec{q}_1}$ $(-x+1/2, y+1/2, -z)$	$\vec{S}_4^{\vec{q}_1}$ $(x+1/2, -y+1/2, -z)$
$(M_x, M_y, 0)$	$(-M_x, -M_y, 0)$	$(M_x, -M_y, 0)$	$(-M_x, M_y, 0)$
$\vec{S}_1^{\vec{q}_2}$ $(x_{1,2}, y_{1,2}, z_{1,2})$	$\vec{S}_2^{\vec{q}_2}$ $(-x_{1,2}+1/2, y_{1,2}+1/2, -z_{1,2})$	$(M_{x_{1,2}}, -M_{y_{1,2}}, 0)e^{2\pi i 0.074}$	
$(M_{x_{1,2}}, M_{y_{1,2}}, 0)$	$(M_{x_{1,2}}, -M_{y_{1,2}}, 0)$		

TABLE I: Complex-valued basis vectors, $\vec{S}_j^{\vec{q}_i}$, of the commensurate and the incommensurate structure for $\vec{q}_1 = (0, 1, 0)$, $\vec{q}_2 = (0, 0.852, 0)$, j substitutes $(x, y, z) = (0.26874, 0.36898, 0)$, $(x_1, y_1, z_1) = (0.26874, 0.36898, 0)$ and $(x_2, y_2, z_2) = (0.7313, 0.6310, 0)$.

ulated structure with a local magnetic arrangement as in the CM phase. The two magnetic orbits are shifted by a relative angle $\phi_R = -19.3(9)^\circ$ and enclose the angles $\Phi_1 = 70(2)^\circ$ and $\Phi_2 = 60(2)^\circ$ with respect to the crystallographic a -axis.

Remarkably, the magnetic moments in the ICM phase point exactly along the direction of the Pt atoms in the basal ab -plane (see Fig. 4c). This suggests that, for temperatures $T_{N_1} < T < T_{N_2}$, the magnetic structure is con-

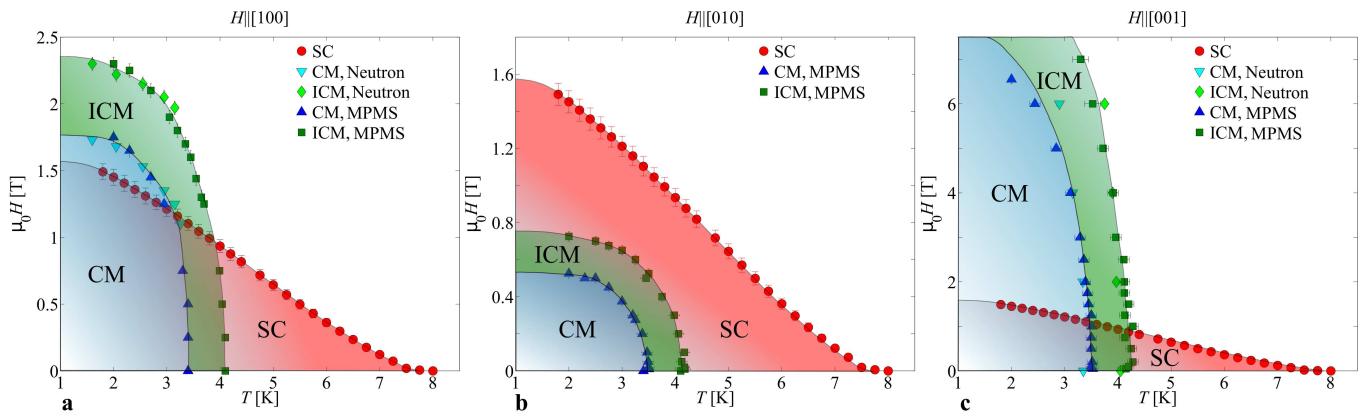


FIG. 5: HT -phase diagram of $\text{Pr}_2\text{Pt}_3\text{Ge}_5$ for (a) $\vec{H}||[100]$, (b) $\vec{H}||[010]$ and (c) $\vec{H}||[001]$. Red denotes the superconducting (SC), green the incommensurate (ICM) and blue the commensurate (CM) phase.

strained by the crystal-field anisotropy. As a compromise between this anisotropy and the Rudermann-Kittel-Kasuya-Yosida (RKKY) exchange the magnetic moments orient along $\Phi = (\Phi_1 + \Phi_2)/2$ in the CM phase below T_{N1} [34–36].

C. Interplay between superconductivity and magnetism

In order to investigate the interplay between superconductivity and magnetism in $\text{Pr}_2\text{Pt}_3\text{Ge}_5$, we explored its HT -phase diagram (in Fig. 5) using a combination of resistivity, magnetization and neutron diffraction measurements [37]. While no anisotropy is found in the superconducting phase, a substantial anisotropy is detected for the magnetic phases. For $\vec{H}||[010]$ magnetic order is most strongly suppressed (see Fig. 5b). This is in agreement with the magnetic refinement (c.f. Fig. 4) and for magnetic moments with a large component along the b -axis, which will be strongly affected by magnetic fields along this direction. Here, both AF phases are fully embedded inside the superconducting phase and the absence of spin-flop transitions upon applying an external magnetic field indicates a strong single-ion anisotropy. In contrast, for $\vec{H}||[001]$ the AF phases survive to much higher fields compared to superconductivity (see Fig 5c). No noticeable changes of the magnetic structures are observed at $\mu_0 H = 6$ T for $\vec{H}||[001]$ and, on a relative error of 0.3%, no anomalies in the intensities of the magnetic reflections are observed upon crossing the superconducting transition. For the hard axis, $\vec{H}||[001]$, the field generates a magnetization out of the basal ab -plane.

For $\vec{H}||[100]$ the AF phases are partly inside and partly outside the superconducting phase (see Fig 5a). The first-order transition from the CM to the ICM phase at low temperatures reaches a saturation at $\mu_0 H \approx 1.73$ T close to the superconducting phase at $\mu_0 H_{c2}(0) \approx 1.6$ T.

However, a simultaneous measurement of the electrical resistivity and the magnetization rules out a collapse of both phases at the same field.

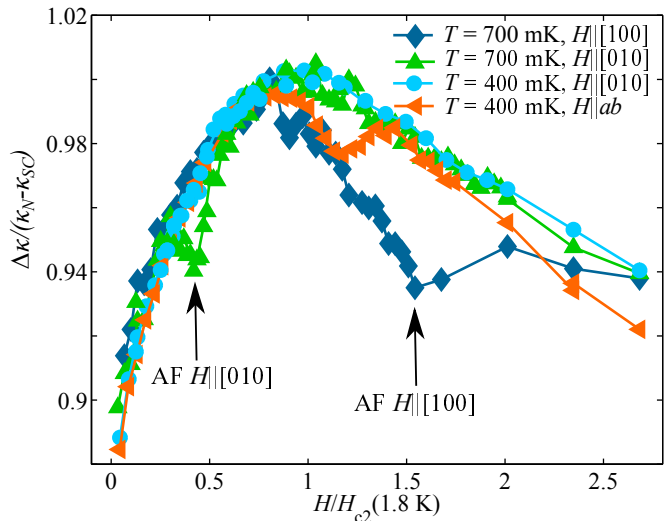


FIG. 6: Field dependence of the normalized electron contribution of the thermal conductivity for different temperatures and field directions.

Field and orientation dependent heat conductivity further identify the interplay between superconductivity and magnetism. Fig. 6 displays $\Delta\kappa/(\kappa_N - \kappa_{SC})$ as a function of the normalized magnetic field, H/H_{c2} , at $T = 400$ and 700 mK and $\vec{H}||[100]$, $[010]$ and ab , respectively. Upon increasing the magnetic field the density of superconducting Cooper pairs is reduced, which causes an increase in $\Delta\kappa/(\kappa_N - \kappa_{SC})$ and results in a maximum at H_{c2} . At the phase boundary between the superconducting and the ICM phase, $\Delta\kappa/(\kappa_N - \kappa_{SC})$ reveals a local minimum. This may be due to the change in rate of electron scattering by spin disorder at the AF phase boundary. At $T = 700$ mK the reduction of the electron scatter-

ing rate is of the order of 6% and less pronounced for lower temperatures (see Fig. 6). We speculate that this reduction is attributed to the reduction of thermal fluctuations at the phase transition for decreasing temperatures. The transition from the ICM to the CM structure is not seen in the thermal conductivity, suggesting that this transition involves only minimal changes that affect the quasi-particles at the Fermi surface.

For $\vec{H}||[010]$, $\Delta\kappa/(\kappa_N - \kappa_{SC})$ is the same as for the other field directions, with the exception for fields close to T_N . This is strong evidence that the electrons that participate in the antiferromagnetic order are not involved with superconductivity. If the same electrons contributed to both superconductivity and antiferromagnetic order, one would expect an increase of thermal conductivity in the antiferromagnetically ordered phase with respect to the purely superconducting phase.

From the field dependent resistivity measurements a Ginzburg-Landau coherence length of $\xi_0 \approx 148 \text{ \AA}$ is estimated using $\mu_0 H_{c2}(0) = \Phi_0/2\pi\xi_0^2$, with Φ_0 the magnetic flux quantum [26, 27]. Since the propagation vectors, \vec{q}_1 and \vec{q}_2 , are much larger than ξ_0^{-1} , the average magnetic fields vanish on the size scale of a Cooper pair. This confirms that superconductivity is not expected to be suppressed by magnetostatic forces [38]. However, our data precludes any microscopic competition of electrons at the Fermi surface to contribute to superconductivity or magnetic order, because magnetic order has no influence on the bulk superconducting state and vice versa.

This is in contrast to the well-studied magnetic superconductors $R\text{Mo}_6\text{S}_8$, $R\text{Mo}_6\text{Se}_8$, $RRh_4\text{B}_4$ and $R\text{Ni}_2\text{B}_2\text{C}$ [8–13]. In these materials the superconducting Cooper pairs are partly broken up by the RKKY-mediated magnetic states [15–17]. Most notable may be $\text{HoNi}_2\text{B}_2\text{C}$ that features several magnetic structures inside the superconducting phase. As a consequence of the interaction between superconductivity and magnetism the HT -phase diagram exhibits a nearly suppressed superconducting phase at the onset of the ICM magnetic transitions [16].

In $\text{Pr}_2\text{Pt}_3\text{Ge}_5$, there is no effect on the magnetic transition temperatures when the material becomes superconducting. Furthermore, thermal conductivity results reveal normal state electrons within the superconducting phase. This suggests that the Fermi surface that is involved in the formation of long-range order through the RKKY interaction does not contribute electrons into the superconducting condensate and remains ungapped below T_c . To our knowledge $\text{Pr}_2\text{Pt}_3\text{Ge}_5$ is the first conventional superconductor in which a competition between superconductivity and magnetism is completely absent.

III. SUMMARY

In summary, thermal conductivity results provides evidence for a large density of normal state electrons within

the superconducting phase of $\text{Pr}_2\text{Pt}_3\text{Ge}_5$ and suggests multigap superconductivity. Neutron diffraction data reveal a second-order phase transition at, $T_{N_2} < T_c$, into a magnetically-ordered phase inside the superconducting phase. For temperatures $T_{N_1} < T \leq T_{N_2}$ and zero field an incommensurate, amplitude modulated non-collinear antiferromagnetic structure with $\vec{q}_2 \approx (0, 0.85, 0)$ is found, for which the magnetic moments are confined in the ab -plane with $\mu(3.5 \text{ K}) \approx 2\mu_B$. With decreasing temperature the magnetic structure transforms, at T_{N_1} , into a commensurate, non-collinear antiferromagnetic structure with $\vec{q}_1 = (0, 1, 0)$ and $\mu(2.1 \text{ K}) \approx 2.3\mu_B$, without any detectable effect on superconductivity. The phase transition at T_{N_1} is of a first-order with a similar moment configuration as in the incommensurate phase.

As the key result of this study, we observe no significant anisotropy of $H_{c2}(T)$ as a function of field direction, but a substantial anisotropy of the magnetic phases for different field directions. The interpenetrating HT -phase diagrams and field dependent thermal conductivity results along different crystal axes demonstrate that superconductivity and magnetism emerge from two separate, completely decoupled mechanisms. Thermal conductivity results suggest that different sheets of the Fermi surface are responsible for the superconducting pairing mechanism and for the RKKY interaction in $\text{Pr}_2\text{Pt}_3\text{Ge}_5$.

ACKNOWLEDGMENTS

We acknowledge the Paul Scherrer Institut for the allocated beam time on DMC, TriCS and TASP at SINQ. In addition, we thank the Swiss National Foundation (grant No. 200021_147071 and 200021_138018) and the European Community's Seventh Framework (FP7/2007-2013), grant No. 290605, COFUND: PSI-FELLOW. M. M. is partly supported by Marie Skłodowska Curie Action, International Career Grant through the European Union and the Swedish Research Council (VR), Grant No. INCA-2014-6426.

* daniel.mazzone@psi.ch

† Present address: KTH Royal Institute of Technology, Electrum 229, SE-16440 Kista, Stockholm, Sweden

‡ Present address: Oakridge National Laboratory, Tennessee, USA

§ michel.kenzelmann@psi.ch

- [1] V. L. Ginzburg, Zh. Eksp. Teor. Fiz. **31**, 202 (1956).
- [2] F. Steglich, J. Arndt, O. Stockert, S. Friedemann, M. Brando, C. Klinger, C. Krellner, C. Geibel, S. Wirth, S. Kirchner, and Q. Si, J. Phys.: Condens. Matter **24**, 294201 (2012).
- [3] G. R. Stewart, Z. Fisk, J. O. Willis, and J. L. Smith, Phys. Rev. Lett. **52**, 679 (1984).

- [4] P. Monthoux, D. Pines, and G. G. Lonzarich, *Nature* **49**, 1177 (2007).
- [5] B. T. Matthias, H. Suhl, and E. Corenzwit, *Phys. Rev. Lett.* **1**, 92 (1958).
- [6] W. Baltensperger, and S. Strässler, *Phys. kondens. Materie* **1**, 20 (1963).
- [7] T. Matsubara, and A. Kontani, *Superconductivity in Magnetic and Exotic Materials, Sixth Taniguchi International Symposium*, Springer-Verlag, Berlin/Heidelberg/New York/Tokyo, 1984, 14-18.
- [8] W. A. Fertig, D. C. Johnston, L. E. DeLong, R. W. McCallum, M. B. Maple, and B. T. Matthias, *Phys. Rev. Lett.* **38**, 987 (1977).
- [9] M. Ishikawa, and Ø. Fisher, *Solid State Commun.* **23**, 37 (1977).
- [10] H. Eisaki, H. Takagi, R. J. Cava, B. Batlogg, J. J. Krajewski, W. F. Peck, Jr., K. Mizuhashi, J. O. Lee, and S. Uchida, *Phys. Rev. B* **50**, 647(R) (1994).
- [11] R. J. Cava, H. Takagi, H. W. Zandbergen, J. J. Krajewski, W. F. Peck Jr., T. Sigrüst, B. Batlogg, R. B. Van Dover, R. J. Felder, K. Mizuhashi, J. O. Lee, O. Eisaki, and S. Uchida, *Nature* **367**, 252 (1994).
- [12] R. J. Cava, H. Takagi, B. Batlogg, H. N. Zandbergen, J. J. Krajewski, W. F. Peck Jr., R. B. Van Dover, R. J. Felder, T. Sigrüst, K. Mizuhashi, J. O. Lee, O. Eisaki, and S. Uchida, *Nature* **367**, 146 (1994).
- [13] L. C. Gupta, *Advances in Physics* **55**, 691 (2006).
- [14] M. B. Maple, *Physica C* **341**, 47 (2000).
- [15] C. T. Wolowiec, B. D. White, and M. B. Maple, *Physica C* **514**, 113 (2015).
- [16] K. H. Müller, and V. N. Narozhnyi, *Rep. Prog. Phys.* **64**, 943 (2001).
- [17] M. B. Maple, *Physica B* **215**, 110 (1995).
- [18] N. H. Sung, C. J. Roh, K. S. Kim, and B. K. Cho, *Phys. Rev. B* **86**, 224507 (2012).
- [19] Y. Nakajima, T. Nakagawa, T. Tamegai, and H. Harima, *Phys. Rev. Lett.* **100**, 157001 (2008).
- [20] Y. Singh, and S. Ramakrishnan, *Phys. Rev. B* **69**, 174423 (2004).
- [21] S. Ramakrishnan, N. G. Patil, A. D. Chinchure, and V. R. Marathe, *Phys. Rev. B* **64**, 064514 (2001).
- [22] S. Skanthakumar, J. W. Lynn, C. Mazumdar, R. Nagarajan, and L. C. Gupta, *Physica B* **241**, 693 (1998).
- [23] S. Noguchi, and K. Okuda, *Physica B* **194**, 1975 (1976).
- [24] J. Rodríguez-Carvajal, *Physica B* **192**, 55 (1993).
- [25] R. Helfand, and R. C. Werthamer, *Phys. Rev.* **147**, 288 (1966).
- [26] R. C. Werthamer, R. Helfand, and P. C. Hohenberg, *Phys. Rev.* **147**, 295 (1966).
- [27] K. Maki, *Phys. Rev.* **148**, 362 (1966).
- [28] C. B. Vining, R. N. Shelton, H. F. Braun, and M. Pelizzone, *Phys. Rev. B* **27**, 2800 (1983).
- [29] Y. Machida, S. Sakai, K. Izawa, H. Okuyama, and T. Watanabe, *Phys. Rev. Lett.* **106**, 107002 (2011).
- [30] A. V. Sologubenko, J. Jun, S. M. Kazakov, J. Karpinski, and H. R. Ott, *Phys. Rev. B* **66**, 014504 (2002).
- [31] E. Boaknin, M. A. Tanatar, J. Paglione, D. Hawthorn, F. Ronning, R. W. Hill, M. Sutherland, L. Taillefer, J. Sonier, S. M. Hayden, and J. W. Brill, *Phys. Rev. Lett.* **90**, 117003 (2003).
- [32] J. Lowell, and J. B. Sousa, *J. Low. Temp. Phys.* **3**, 65 (70).
- [33] L. Durivault, F. Bourée, B. Chevalier, G. André, and J. Etourneau, *J. Magn. Magn. Mater.* **246**, 366 (2003).
- [34] M. A. Rudermann, and C. Kittel, *Phys. Rev.* **96**, 99 (1954).
- [35] T. Kasuya, *Prog. Theor. Phys.* **16**, 45 (1957).
- [36] K. Yosida, *Phys. Rev.* **106**, 893 (1957).
- [37] In agreement with earlier reports the signal of the magnetization measurements is dominated by the response of the AF phases for fields above $\mu_0 H \approx 50$ mT [18]. All states were prepared in zero field-cooled mode.
- [38] T. Matsubara, and A. Kontani, *Superconductivity in Magnetic and Exotic Materials, Sixth Taniguchi International Symposium*, Springer-Verlag, Berlin/Heidelberg/New York/Tokyo, 1984, 4,104.